International Journal of Scientific Research in Mathematical and Statistical Sciences
Vol.**11**, Issue.**1**, pp.**34-42**, February **2024**
E-ISSN: 2348-4519
Available online at: www.isroset.org

Research Article

Fractional Mathematical Modelling of Blood Flow Dynamics in Arterial Segments for The Treatment of Cardiovascular Diseases

Mukhtar Abubakar Maiwada[1*], Adamu Garba Tahiru[2], Isah Abdullahi[3], Idris Babaji Muhammad[4]

[1,2,4]Dept. of Mathematical Sciences, Bauchi State University, Gadau, Bauchi, Nigeria
[3]Dept. of Mathematical Sciences, Abubakar Tafawa Balewa University, Bauchi, Nigeria

**Corresponding Author: isahabdullahi7474@gmail.com, Tel: +2347039747474*

Received: 01/Jan/2024; **Accepted**: 02/Feb/2024; **Published**: 29/Feb/2024

Abstract—This study presents a comprehensive numerical analysis of electro-magneto-hydrodynamic (EMHD) blood flow through arterial segments with a focus on potential implications for cardiovascular therapeutics. The investigation encompasses the impact of various parameters, including electrokinetic width, particle concentration, chemical reaction, and heat source, on blood velocity, nanoparticle velocity, and concentration profiles. The findings reveal the potential for enhanced targeting and delivery of therapeutic nanoparticles through the manipulation of magnetic fields, indicating promising prospects for targeted drug delivery in cardiovascular disease treatments. Additionally, the complex interplay between chemical reactions and blood flow dynamics underscores the need for a refined understanding of these interactions for potential therapeutic interventions. The study also highlights the significance of considering heat transfer dynamics in EMHD blood flow, offering insights into potential implications for cardiovascular health and disease management. Overall, the numerical analysis provides valuable insights into the rheological behaviour of blood and its potential applications in cardiovascular therapeutics, emphasizing the need for further research in this critical area of study.

Keywords— Nano Particles, Arterial Segment, Cardiovascular Diseases, Time-Fractional Derivative

1. Introduction

In recent decades, the study of bio-fluid dynamics, particularly the rheological behavior of blood, has garnered significant attention from researchers. The recognition of blood as a non-Newtonian fluid, characterized by complex dynamic processes influencing shear-thinning, viscoelasticity, and thixotropy, has profound implications for understanding its crucial role in maintaining life. Blood flow is essential for transporting oxygen, nutrients, and removing metabolic waste from cells, making it a critical factor in overall physiological health [1,2,3,4,5,6,7]. Cardiovascular ailments like Atherosclerosis, Aneurysms, and Stenosis contribute significantly to both fatalities and health issues worldwide. A comprehensive comprehension of blood circulation via simulation is indispensable for making well-informed choices in managing such cardiovascular disorders. Blood is a mixture of blood cells within plasma, where plasma accounts for 55% of the blood's liquid portion, mainly consisting of water (making up 92% by volume).

The plasma also contains dissipated proteins, glucose, mineral ions, hormones, and various blood cells, including red blood cells, white blood cells, and platelets. Red blood cells, in particular, contribute to the creation of a magnetic field on the walls of arteries due to their negative charge carriers, further emphasizing the complexity of blood flow dynamics [6,7,8,9]. To accurately model and simulate the rheological response of blood under different physiological conditions, researchers emphasize the need for an accurate constitutive mathematical model. This model is crucial for meaningful hemodynamic simulations that can aid in the understanding and treatment of cardiovascular diseases [10].

Despite the considerable amount of research conducted on blood as a non-Newtonian fluid and the crucial need for precise modelling in hemodynamic simulations, there remains a gap in understanding how fractional calculus can be appropriately utilized to capture the intricate dynamics of blood flow. Fractional calculus has garnered attention across a spectrum of scientific, engineering, biological, and medical contexts. [11,12]. However, its specific application to describe the rheological behavior of non-Newtonian fluids, especially blood, remains an area that requires further exploration. The existing literature highlights the Jeffrey model as a noteworthy framework among non-Newtonian fluids, incorporating convective derivatives to address

phenomena like relaxation and retardation time [13,14,15,16,17,18,19,20]. Nevertheless, there has been an insufficient examination of how fractional calculus, particularly in combination with the Jeffrey model, can be utilized. This study seeks to address this deficiency by examining how fractional calculus, specifically fractional derivatives, can improve the precision of the Jeffrey model in simulating blood flow. The research endeavours to advance our comprehension of blood's rheological properties, offering valuable perspectives that can enhance decision-making in cardiovascular disease management.

2. Related Work

The study by [21] has laid a foundation for investigating the dynamics of blood flow through arterial segments. Their work primarily focused on the interactions between heat transfer, thermal radiation, and chemical reactions, providing valuable insights into the physiological processes involved. However, as identified by the current research, there is a recognized need for a refined mathematical model that incorporates fractional derivatives to achieve a more comprehensive understanding. Several studies have delved into aspects of blood flow modelling, each contributing unique perspectives to the complex interplay of factors influencing arterial dynamics.[22] explored the role of heat transfer in arterial blood flow, shedding light on the thermal aspects of this intricate system. Furthermore, the work of [23] addressed the impact of chemical reactions on blood composition, emphasizing the biochemical dimension of arterial flow.

However, to date, there remains a gap in the literature regarding a unified model that seamlessly integrates heat transfer, thermal radiation, and chemical reactions, considering the fractional derivatives associated with arterial behavior. The proposed research aims to bridge this gap by refining and extending the groundwork laid by [21]. In doing so, it aims to contribute to a more detailed and comprehensive comprehension of the integrated factors impacting blood flow within arterial segments. While existing studies have made valuable contributions to the understanding of various aspects of blood flow dynamics, the current research strives to advance this knowledge by proposing a modified mathematical model that addresses the identified limitations in the work of [21] and integrates fractional derivatives for a more accurate representation of arterial behavior.

3. Methodology

Fundamentally, when analysing fluid dynamics, one takes into account the core equations regulating the uncompressible flow of fluid within segmented arteries, especially concerning drug delivery for cancer therapy. These equations encompass the momentum equation, the nanoparticle equation, the energy equation, and the concentration equation.

$$\left.\begin{aligned}&\rho\frac{\partial\bar{u}_f}{\partial\bar{t}}=\frac{\partial\bar{p}}{\partial\bar{z}}+\frac{\mu}{1+\lambda}\left[\frac{1}{r}\frac{\partial}{\partial\bar{r}}\left(\bar{r}\frac{\partial\bar{u}_f}{\partial\bar{r}}\right)\right]+\\&K_S N_p\left(\overline{u_f}-\overline{u_p}\right)\\&+P_C E_Z-\bar{\delta}\beta^2\bar{u}_f+\\&gB_T\left(\bar{T}-T_\omega\right)+gB_C\left(\bar{C}-C_\omega\right)\end{aligned}\right\} \quad (1)$$

$$M\frac{\partial\overline{u_p}}{\partial\bar{t}}+\overline{K_S}\left(\overline{u_f}-\overline{u_p}\right) \quad (2)$$

$$\rho C_p\frac{\partial\bar{T}}{\partial\bar{t}}=K\left[\frac{1}{\bar{r}}\frac{\partial}{\partial\bar{r}}\left(r\frac{\partial\bar{T}}{\partial\bar{r}}\right)\right]-\frac{\partial q_r}{\partial\bar{r}}+Q_m \quad (3)$$

$$\left.\begin{aligned}&\frac{\partial\bar{C}}{\partial\bar{t}}=D_M\left[\frac{1}{\partial\bar{r}}\frac{\partial}{\partial\bar{r}}\left(r\frac{\partial\bar{c}}{\partial\bar{r}}\right)\right]+\\&\frac{D_M K_T}{T_0}\left[\frac{1}{r}\frac{\partial}{\partial\bar{r}}\left(r\frac{\partial\bar{T}}{\partial\bar{r}}\right)\right]-K_0\left(\bar{C}-C_\omega\right)\end{aligned}\right\} \quad (4)$$

Here ρ is the fluid density, $\frac{\partial}{\partial t}$ is the material time derivative, $\bar{u}_f-\bar{u}_p$ is the relative velocity and $\bar{K}_s$ is the stoke constant, r is the radius of the artery, β_c is the applied uniform magnetic field N_p is the number of magnetic nanoparticle per unit volume, $\bar{T}$ is the temperature, $\bar{C}$ is the Concentration, μ is the dynamic viscosity of the fluid, and E_z is the external electric force Imposed at the arterial segment wall. M is the mass of single particle u_f-u_p is the relative velocity and $\bar{K}_s$ is the stoke constant. From Equation (1) and (3), we define the pressure gradient and heat radiation respectively as follows:

$$\frac{\partial\bar{p}}{\partial\bar{z}}=\overline{a_0}+\overline{a_1}\cos\left(\varpi_p\bar{t}\right) \quad (5)$$

$$\frac{\partial q_r}{\partial\bar{r}}=4\alpha^2\left(\bar{T}-T_0\right) \quad (6)$$

The corresponding initial and boundary conditions are;

$$\left.\begin{aligned}&\left(\bar{r},0\right)=0,\frac{\partial\bar{u}\left(\bar{r},0\right)}{\partial\bar{t}}=0,\bar{u}\left(1,\bar{t}\right)=0,\\&\bar{u}\frac{\partial\bar{u}\left(0,t\right)}{\partial\bar{r}}=0,\bar{T}\left(\bar{r},t\right)=T_\omega,\bar{c}\left(\bar{r},t\right)=C_\omega,\\&\frac{\partial\bar{T}\left(0,\bar{t}\right)}{\partial\bar{r}}=0,\frac{\partial\bar{c}\left(0,t\right)}{\partial\bar{r}}=0\end{aligned}\right\} \quad (7)$$

$$\left.\begin{aligned}\nabla^2\bar{\varphi}(\bar{r}) &= \frac{1}{\bar{r}}\frac{\partial}{\partial\bar{r}}\left(\bar{r}\frac{\partial\bar{\varphi}(\bar{r})}{\partial\bar{r}}\right)+\\ \frac{1}{\bar{r}^2}\left(\bar{r}\frac{\partial^2\bar{\varphi}(\bar{r})}{\partial\bar{z}}\right) &= \frac{\bar{\rho}_e(\bar{r})}{\varepsilon}\end{aligned}\right\} \quad (8)$$

Equation (7) is known as the Boltzmann equation with the boundary conditions and the net charge density given as;

$$\bar{\varphi}(1)=\varphi_\omega, \qquad and \qquad \frac{\partial\bar{\varphi}}{\partial\bar{r}}=0, at \qquad r=0$$

$$\bar{\rho}_e(\bar{r})=e_0\left(n^+-n^-\right)=\frac{-2z_0^2e_0n_0\bar{\varphi}(\bar{r})}{k_gT_C}$$

Here ρ_e is the dielectric constant, z_0, n_0, e_0, k_g , n^+ and n^- are the ion valence, concentration of ions, the electronic charge, the Boltzmann constant the local absolute temperature of the fluid, the density number of cations and anions, respectively.

Using Debye–Huckelparameter

$$\bar{k}^2=\frac{2z_0^2c_0^2n_0\bar{\varphi}(\bar{r})}{ck_gT_0}$$

and linearized the Boltzmann equation (8), we get a potential equation as

$$\frac{1}{\bar{r}}\frac{\partial}{\partial\bar{r}}\left(\bar{r}\frac{\partial\bar{\varphi}(\bar{r})}{\partial\bar{r}}\right)=\bar{k}^2\bar{\varphi}(\bar{r}) \quad (9)$$

The Caputo-Fabrizio derivative with fractional order $\alpha\epsilon(0,1)$ is define as:

$${}^{CF}D_t^\alpha f(t)=\frac{M(\alpha)}{1-\alpha}\int_0^1 f(\tau)\exp\left[\frac{-\alpha(t-\tau)}{1-\alpha}\right]d\tau \quad (10)$$

The dimensionless parameters that are under consideration in the context of dimensionless initial and boundary conditions are:

$$\left\{\begin{aligned}&u_f=\frac{\bar{u}_f}{u_0}, u_p=\frac{\bar{u}_p}{u_0}, r=\frac{\bar{r}}{R_0}, z=\frac{\bar{z}}{R_0},\\ &t=\bar{\omega}_p\bar{t}, P=\frac{\bar{P}R_0^2}{\mu u_0}a_0=\frac{\bar{a}_0R_0}{\mu u_0},\\ &a_1=\frac{\bar{a}_1R_1^2}{\mu u_0}, S=\frac{\bar{S}R_0^2}{\mu u_0}, \varphi=\frac{\bar{\varphi}}{\bar{\varphi}_\omega}\end{aligned}\right. \quad (11)$$

On substituting equation (11) into equations (1)-(9) and simplifying with the aid of definition (10), we obtain:

$$\left.\begin{aligned}&\beta^2D_t^\alpha u_f(r,t)=f(t)+\\ &\frac{1}{1+\lambda}\left[\frac{1}{r}\frac{\partial}{\partial r}\left(r\frac{\partial u_f}{\partial r}\right)\right].\\ &+R_c\left(u_p-u_f\right)-\\ &M^2u_fk^2\varphi(r)G_r\theta+G_c\phi\end{aligned}\right\} \quad (12)$$

$$\beta^2GD_t^\alpha u_p(r,t)=u_f(r,t)-u_p(r,t) \quad (13)$$

$$D_t^\alpha\theta(r,t)=\frac{1}{p_e}\left[\frac{1}{r}\frac{\partial}{\partial r}\left(r\frac{\partial u_f}{\partial r}\right)\right].-R\theta+Q_m \quad (14)$$

$$\left.\begin{aligned}D_t^\alpha\phi(r,t)=\frac{1}{S_c}&\left[\left[\frac{1}{r}\frac{\partial}{\partial r}\left(r\frac{\partial u_f}{\partial r}\right)\right]\right]-\\ &S_r\left[\left[\frac{1}{r}\frac{\partial}{\partial r}\left(r\frac{\partial u_f}{\partial r}\right)\right]\right]-k_c\phi\end{aligned}\right\} \quad (15)$$

Where $f(t)=\frac{-\partial p}{\partial t}=a_0+a_1\cos(\omega t)$

$$\left\{\begin{aligned}&u_f(1,t)=0, u_p(1,t)=0\\ &\theta(1,t)=0, \phi(1,t)=0\\ &\frac{\partial u(0,t)}{\partial r}=0, \frac{\partial\theta(0,t)}{\partial r}=0, \frac{\partial\phi(0,t)}{\partial r}=0\end{aligned}\right. \quad (16)$$

$$R_e=\frac{R_0u_0}{\nu}, Ha=B_0R_0\sqrt{\frac{\sigma}{p\nu}}, Da=\frac{k_p}{R_0^2}, P_c=\frac{KNR_0^2}{\mu},$$

$$Gr=\frac{gB_T\left(\bar{T}_\omega-T_\infty\right)R_0^3}{\nu^2}, Gc=\frac{gB_c\left(\bar{C}_\omega-C_\infty\right)R_0^3}{\nu^2},$$

$$P_m=\frac{mu_0}{kR_0}, P_r\frac{\mu c_p}{k}, P_e=R_eP_r, R=\frac{4\alpha_2^2R_0^2}{k}$$

$$Sc=\frac{\nu}{D_m}, \frac{D_mK_T\left(T_W-T_\infty\right)}{\nu T_\infty\left(C_W-C_\infty\right)}, K_c=\frac{k_0\nu}{u_0^2}$$

The Reynolds number, the Hartmann Number, the Darcy parameter, the particle concentration parameter, the thermal Grashof number, the mass Grashof number, the particle mass parameter the Prandlt number, the Peclet number, the thermal radiation parameter, Sc the Schmidt number, the Soret number, and the chemical reaction parameter respectively. Now by applying Laplace transforms on equation (12)-(15), we have

$$\left.\begin{aligned}\frac{\beta^2 s u_f^*(r,s)}{(1-\alpha)s+\alpha} &= f(s)\frac{1}{1+\lambda}\\ &\left[\frac{1}{r}\frac{\partial}{\partial r}\left(r\frac{\partial u_f^*(r,s)}{\partial r}\right)\right].\\ &+R_c\left(u_p(r,s)-u_f^*(r,s)\right)\\ &-M^2 u_f^*(r,s)k^2\varphi(r)\\ &+G_r\theta^*(r,s)+G_c\phi^*(r,s)\end{aligned}\right\} \quad (17)$$

$$\frac{\beta^2 S u_f^*(r,s)}{(1-\alpha)s+\alpha} = u_p(r,s)-u_f^*(r,s) \quad (18)$$

$$\left.\begin{aligned}\frac{s\theta^*(r,s)}{(1-\alpha)s+\alpha} &= \frac{1}{p_e}\left[\frac{1}{r}\frac{\partial}{\partial r}\left(r\frac{\partial u_f^*(r,s)}{\partial r}\right)\right].\\ &-R\theta^*(r,s)+\frac{Q_m}{s}\end{aligned}\right\} \quad (19)$$

$$\left.\begin{aligned}\frac{s\phi^*(r,s)}{(1-\alpha)s+\alpha} &= \frac{1}{s_c}\left[\left[\frac{1}{r}\frac{\partial}{\partial r}\left(r\frac{\partial\theta*(r,s)}{\partial r}\right)\right]\right]\\ &-s_r\left[\left[\frac{1}{r}\frac{\partial}{\partial r}\left(r\frac{\partial\theta*(r,s)}{\partial r}\right)\right]\right]-\frac{k_c}{s}\phi^*\theta*(r,s)\end{aligned}\right\} \quad (20)$$

From equation (18), we have

$$u_p^*(r,r)=\left[\frac{(1-\alpha)s+\alpha}{\beta^2 GS+(1-\alpha)S+\alpha}\right]u_f^*(r,s) \quad (21)$$

Substituting equation (21) into (17), we have

$$\left.\begin{aligned}&\left[\frac{\beta^2 S+R\beta^2 GS+M^2\left[(1-\alpha)S+\alpha\right]}{\left[(1-\alpha)S+\alpha\right]}\right]\\ &u_f^*(r,s)=f(s)\frac{1}{1+\lambda}\\ &\left[\frac{1}{r}\frac{\partial}{\partial r}\left(r\frac{\partial u_f^*(r,s)}{\partial r}\right)\right].\frac{k^2}{S}\varphi(r)\\ &+G_r\theta^*(r,s)+G_c\phi^*(r,s)\end{aligned}\right\} \quad (22)$$

From equation (19) and (20) we have the following

$$\left.\begin{aligned}&\left[\frac{s+R_c\left[(1-\alpha)s+\alpha\right]}{(1-\alpha)S+\alpha}\right]\theta^*(r,s)=\\ &\frac{1}{p_e}\left[\frac{1}{r}\frac{\partial}{\partial r}\left(r\frac{\partial u_f^*(r,s)}{\partial r}\right)\right].-\\ &R\theta^*(r,s)+\frac{Q_m}{s}\end{aligned}\right\} \quad (23)$$

$$\left.\begin{aligned}&\left[\frac{s+k_c\left[(1-\alpha)s+\alpha\right]}{(1-\alpha)S+\alpha}\right]\phi^*(r,s)=\\ &\frac{1}{S_c}\left[\left[\frac{1}{r}\frac{\partial}{\partial r}\left(r\frac{\partial\theta*(r,s)}{\partial r}\right)\right]\right]-s_r\\ &\left[\left[\frac{1}{r}\frac{\partial}{\partial r}\left(r\frac{\partial\theta*(r,s)}{\partial r}\right)\right]\right]-\frac{k_c}{s}\phi^*\theta*(r,s)\end{aligned}\right\} \quad (24)$$

Now applying finite Henkel transform on equations (20) - (24), and simplifying, we obtain:

$$\left.\begin{aligned}u_f^{**}(\gamma_n,s) &= \left[\frac{(1+\lambda)\left[(1-\alpha)s+\alpha\right]}{\Pi(\gamma_{n,}s)}\right]\\ &\left[f(s)\frac{J_1(\gamma_n)}{\gamma_n}-\frac{k^2}{S}\frac{\gamma_n J_1(\gamma_n)}{\gamma_n}\right.\\ &\left.+G_r\theta^{**}(\gamma_n,s)+G_c\phi^{**}(\gamma_n,s)\right]\end{aligned}\right\} \quad (25)$$

$$\theta^{**}(\gamma_n,s)=\left[\frac{\left[(1-\alpha)s+\alpha\right]p_e}{\Gamma_n(\gamma_n,s)}\right]\frac{Q_m}{s}\frac{J_1(\gamma_n)}{\gamma_n} \quad (26)$$

$$\left.\begin{aligned}\phi^{**}(\gamma_n,s) &= \left[\frac{S_c S_r\gamma_n^2\left[(1-\alpha)s+\alpha\right]}{\Phi(\gamma_n,s)}\right]\\ &\left[\frac{\left[(1-\alpha)s+\alpha\right]p_e}{\Gamma_n(\gamma_n,s)}\right]\frac{Q_m}{s}\frac{J_1(\gamma_n)}{\gamma_n}\end{aligned}\right\} \quad (27)$$

By substituting equation (26) and equation (27) into equation (25), we have;

$$u_f^{**}(\gamma_n,s)=\left\{\begin{array}{l}\left[\frac{(1+\lambda)[(1-\alpha)s+\alpha]}{\Pi(\gamma_{n,}S)}\right]\\ \left[\begin{array}{l} f(s)\frac{j_1(\gamma_n)}{\gamma_n}-\frac{k^2}{s}\frac{\gamma_n J_1(\gamma_n)}{\gamma_n}+\\ \left[\begin{array}{l} G_r-\\ G_c\\ \left(\left[\frac{S_c S_r\gamma_n^2[(1-\alpha)s+\alpha]}{\Phi(\gamma_n,s)}\right]\right)\end{array}\right]\end{array}\right]\\ \left[\left[\frac{[(1-\alpha)s+\alpha]p_e}{\Gamma_n(\gamma_n,s)}\right]\frac{Q_m}{s}\frac{J_1(\gamma_n)}{\gamma_n}\right]\end{array}\right\} \quad (28)$$

$$\Pi(\gamma_{n,}S)=C_n+d_n\alpha$$

where

$$C_n=\left[(1+\lambda)\beta^2(1+R_cG)+M^2(1-\alpha)+\gamma_n^2(1-\alpha)\right]+\gamma_n^2(1-\alpha)$$

$$d_n=M^2(1+\lambda)+\gamma_n^2$$

$$\Gamma_n(\gamma_n,s)=a_ns+b_n\alpha$$

where

$$a_n=p_e(1+R_C(1-\alpha))+\gamma_n^2(1-\alpha)$$

$$b_n=R_cp_e+\gamma_n^2$$

$$\Phi(\gamma_n,S)=e_ns+f_n\alpha$$

Here

$$e_n=S_c(1+k_c(1-\alpha))+\gamma_n^2(1-\alpha)$$

$$f_n=k_cS_c+\gamma_n^2$$

Now by applying the invers Henkel transform to equations (26)- (28)

$$\theta(r,s)=\left[\frac{[(1-\alpha)S+\alpha]p_e}{\Gamma_n(r,s)}\right]\frac{Q_m}{s}\Omega(r) \quad (29)$$

$$\phi(r,s)=\left\{\begin{array}{l}\left[\frac{S_cS_r\gamma_n^2[(1-\alpha)S+\alpha]}{\Phi(r,s)}\right]\\ \left[\frac{[(1-\alpha)s+\alpha]p_e}{\Gamma_n(r,s)}\right]\frac{Q_m}{s}\Omega(r)\end{array}\right\} \quad (30)$$

$$u(r,s)=\left\{\begin{array}{l}\left[\frac{(1+\lambda)[(1-\alpha)s+\alpha]}{\Pi(r,s)}\right]\\ \left[\begin{array}{l} F(s)\Delta(r)-\frac{1}{s}\Lambda(r)+(G_r\\ -G_c)\left[\frac{S_cS_r\gamma_n^2[(1-\alpha)s+\alpha]}{\Phi(r,s)}\right]\end{array}\right]\\ \left[\frac{[(1-\alpha)s+\alpha]p_e}{\Gamma_n(r,s)}\right]\left(\frac{Q_m}{s}\Omega(r)\right)\end{array}\right\} \quad (31)$$

where

$$\Delta(r)=2\sum_{n=1}^{\infty}\frac{J_0(\gamma_n,r)}{\gamma_nJ_1(\gamma_n)}$$

$$\Lambda(r)=2\sum_{n=1}^{\infty}\frac{k\gamma_n^2}{\gamma_n^2+k^2}\frac{J_0(\gamma_n,r)}{\gamma_nJ_1(\gamma_n)}$$

The inverse Laplace form of equations (29) to (31) was taken with the aid of Gerby-Stefan's Algorithm and the results were simulated graphically with the aid of MATCARD software as shown in the next section.

4. Results and Discussion

In this section, we showcased and deliberated upon the numerical outcomes and simulations depicted graphically for the electro-magneto-hydrodynamic blood flow through arterial segments influenced by a magnetic field.

The Velocity of Blood

In this section, we discuss the impact of various blood flow parameters on blood velocity. Figure 1 illustrates that a higher value of electrokinetic width results in increased electromagnetic strength, suggesting a resistive effect on blood velocity. Additionally, Figure 1 demonstrates that widening the electrokinetic widths significantly decreases blood flow velocity, with higher velocity observed at the center compared to the arterial wall vicinity. Examining Figure 2, we observe the influence of the particle concentration parameter on blood flow velocity, indicating no significant effect on velocity. Likewise, Figure 3 reveals that a higher value of the chemical reaction parameter enhances blood velocity, with lower velocity at the arterial wall compared to the center. Furthermore, Figure 4 illustrates that a higher value of the metabolic heat source has a resistive impact on blood velocity, resulting in reduced velocity from the center to the arterial wall as the heat source parameter increases.

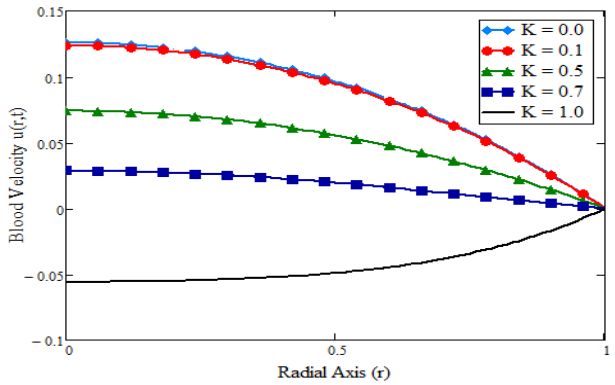

Figure 1: *Blood velocity for various values of Kinetic width (K)*

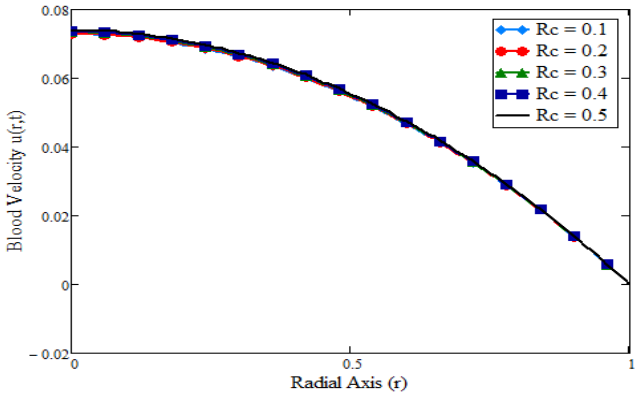

Figure 2: *Blood velocity for various values of Particle concentration parameter (Rc)*

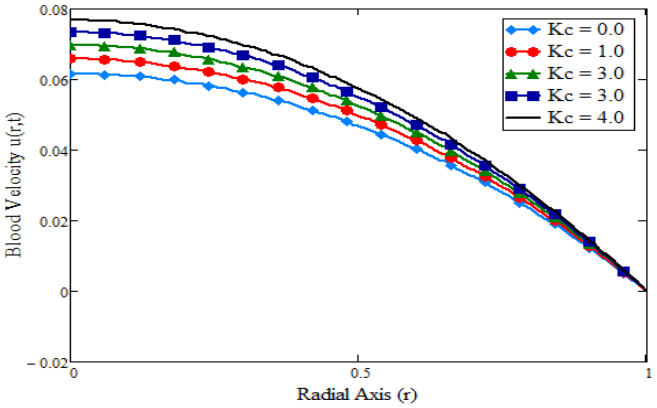

Figure 3: *Blood velocity for various values of chemical reaction parameter (Kc)*

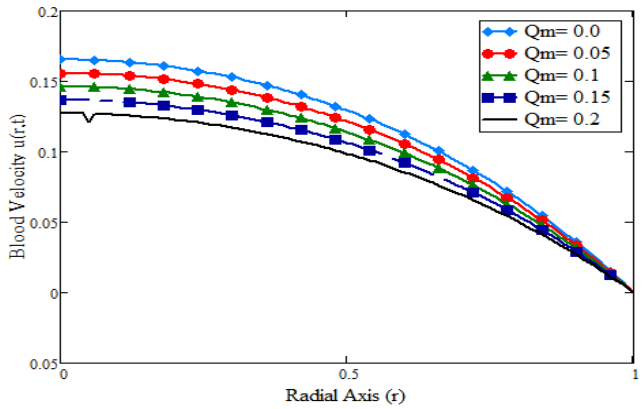

Figure 4: *Blood velocity for various values of heat source parameter (Qm)*

The Nanoparticles Velocity

The manipulation of targeted magnetic nanoparticles is easily achieved by applying a magnetic field, which enhances particle capture at sites affected by cardiovascular diseases. Magnetic drug targeting appears to be more effective for lower values of K. The presence of kinetic widths introduces an additional magnetic field form that acts externally on the body, significantly affecting both blood velocity and nanoparticle velocity. Consequently, this results in an increased magnetic force on the particles, leading to reduced particle motion, as shown in Figure 5. With increasing kinetic widths, the decrease in blood velocity is more pronounced in the arterial wall than at the center due to the interaction between blood flow and magnetic particles. This interaction, known as the Lorentz force, tends to diminish the motion of magnetic nanoparticles. Therefore, the magnetic field plays a crucial role in regulating both blood velocity and the efficiency of nanoparticle capture for targeted drug delivery in specific locations during cardiovascular disease treatments. The findings suggest that an increase in kinetic widths (K) enables nanoparticles to align more effectively with the magnetic field toward the diseased site, as depicted in Figure 6. Additionally, Figure 6 shows that the particle concentration parameter of nanoparticle velocity has no discernible effect on the flow.

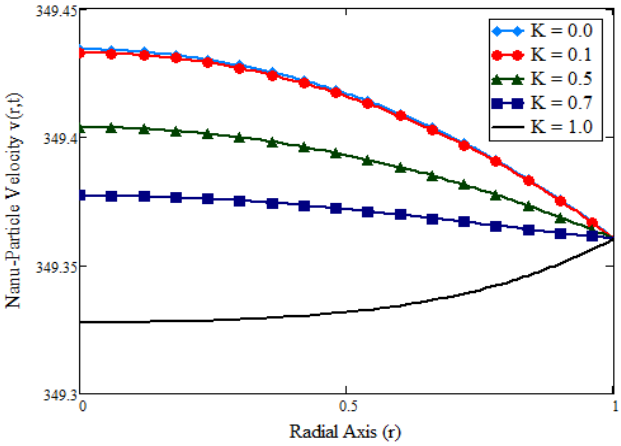

Figure 5: *Nano-Particles velocity for various values of Kinetic width (K)*

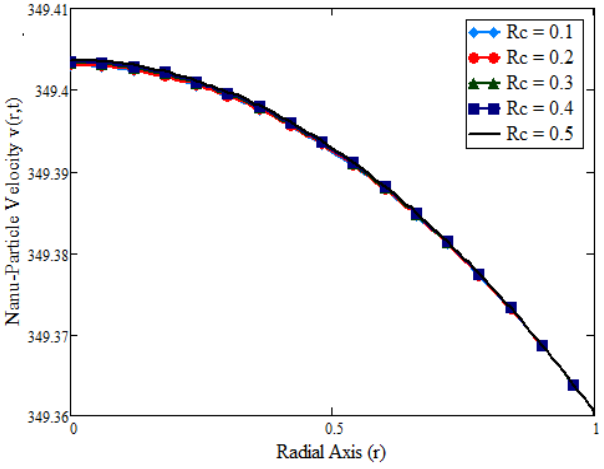

Figure 6: *Nano-Particles velocity for various values of Particle concentration parameter*

The Concentration Profile

In this section, we visually depict the numerical outcomes of the concentration profile in electro-magneto-hydrodynamic (EMHD) blood. Figures 8 and 9 demonstrate that the impact of kinetics widths and particle concentration parameter on the concentration profile is indistinguishable, with no discernible separation between the bars. Figure 10 distinctly illustrates that an elevation in the chemical reaction parameter correlates with an increased concentration profile. The figure indicates that as the chemical reaction values rise, the concentration gradually increases. However, this effect diminishes as it progresses from the center of the artery towards the arterial wall, with the concentration reaching a notably high level at the arterial wall.

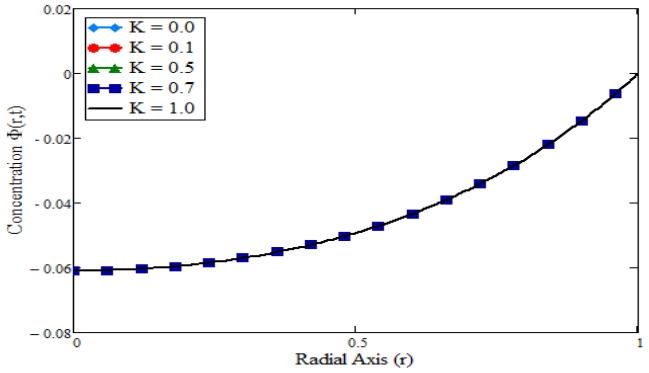

Figure 8; *Concentration for various values of kinetic width (K)*

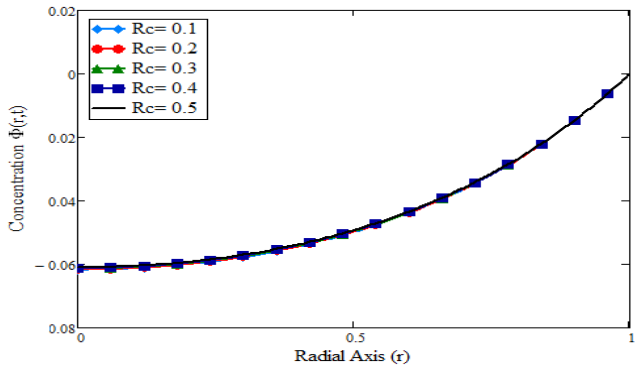

Figure 9; *Concentration for various values of Particle concentration parameter (Rc)*

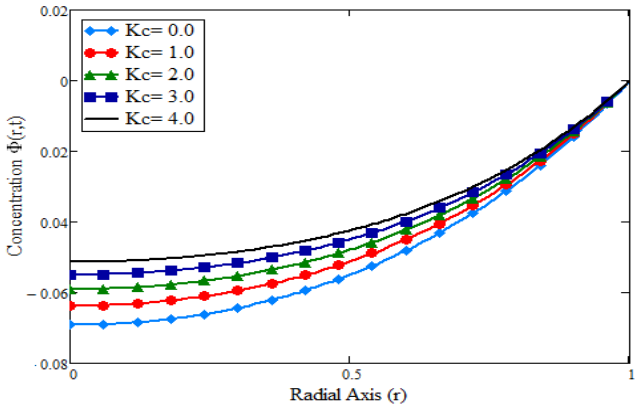

Figure 10: Concentration for various values of chemical reaction parameter (Kc)

The Temperature Profile

In this section, we visually depict and discuss the numerical results concerning the heat dynamics in electro-magneto-hydrodynamic (EMHD) blood flow. Figure 11 is employed to illustrate how changes in kinetic widths influence the temperature profile of EMHD blood flow, showing that higher values of kinetic widths lead to lower temperatures. Figure 12 indicates that alterations in the particle concentration parameter do not visibly impact the temperature of the blood flow. Moreover, Figure 13 clearly shows that an increase in the heat source leads to a rise in the temperature distribution of the blood.

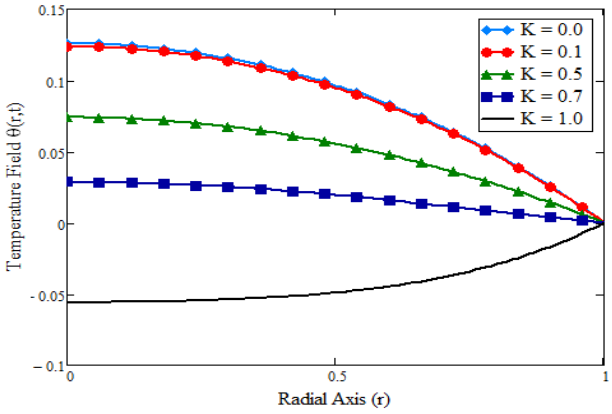

Figure 11: *Temperature field for various values of kinetic width (K)*

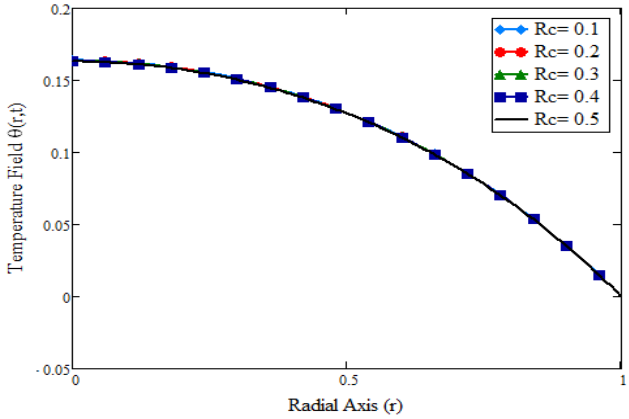

Figure 12; *Temperature for various values of Particle concentration parameter (Rc)*

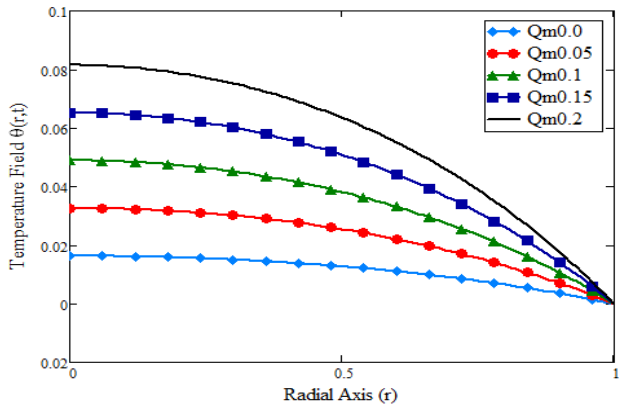

Figure 13; *Temperature for various values of heat source (Qm)*

5. Conclusion

The study primarily focuses on presenting and discussing numerical results and simulations related to the electro-magneto-hydrodynamic blood flow through arterial segments with a magnetic field. it discusses the impact of various blood flow parameters on blood velocity, such as electrokinetic width, particle concentration parameter, chemical reaction parameter, and metabolic heat source. The study also emphasizes the need for a refined mathematical model that incorporates fractional derivatives to achieve a more comprehensive understanding of blood flow dynamics. The general findings from the study revealed that:

1. The manipulation of targeted magnetic nanoparticles through the use of a magnetic field has the potential to enhance particle capture at diseased sites during cardiovascular disease treatments, indicating the promise of magnetic drug targeting for improved therapeutic outcomes.
2. The influence of kinetics widths introduces an additional magnetic field form that acts externally on the body, significantly impacting both blood velocity and nanoparticle velocity, highlighting the crucial role of magnetic fields in controlling both blood velocity and the capturing efficiency of nanoparticles for targeted drug delivery in specific locations during cardiovascular disease treatments.
3. An increase in kinetic widths (K) enables nanoparticles to more effectively align with the magnetic field toward the diseased position, suggesting the potential for improved targeting and delivery of therapeutic nanoparticles in specific areas of the cardiovascular system.
4. The impact of chemical reaction parameters on blood velocity and concentration profiles indicates the complex interplay between chemical reactions and blood flow dynamics, emphasizing the need for a comprehensive understanding of these interactions for potential therapeutic interventions. The findings suggest that variations in the heat source parameter have a discernible effect on the temperature distribution of the blood, highlighting the importance of considering heat transfer dynamics in the context of electro-magneto-hydrodynamic blood flow for potential implications in cardiovascular health and disease management.

Availability of Data and Materials:
Not applicable

Conflict of Interest:
The authors declare that there are no conflicts of interest related to the study. This is an important declaration to ensure transparency and to address any potential biases that could arise from financial or personal relationships.

Funding:
The study received no external support.

Authors' Contributions Statement:
All authors contributed equally to the work and approved the final version of the manuscript.

Acknowledgment:
The authors gratefully acknowledged the reviewers and the Editor in-chief for their comments and necessary suggestions.

References

[1] S. Morovec and D. Liepsch, "Rheology of blood flow," Journal of Biomechanics, vol.**16**, no.**9**, pp. **665-670, 1983**.
[2] P. Chaturani and C. Pannalagar, "Rheology of blood flow," Journal of Biomechanics, vol.**18**, no. **3**, pp.**159-167, 1985.**
[3] J. Janela and A. Moura, "Blood flow simulation in the human aorta," Journal of Biomechanics, vol.**43**, no.**12,** pp.**2345-2352, 2010**.
[4] J. Chen and X. Lu, "Numerical simulation of blood flow in the human aorta," Journal of Biomechanics, vol.**37**, no.**4**, pp.**487-494, 2004**.
[5] J. Bernsdorf and Y. Wang, "Blood flow simulation: a computational tool for clinical decision support," Journal of Healthcare Engineering, vol.**1,** no.**3**, pp.**343-364, 2009.**
[6] P. K. Mandal, "Blood flow simulation in the human aorta: a review," Journal of Medical Engineering & Technology, vol.**39**, no.**6**, pp.**319-327, 2015**.
[7] S. Padma, K. Srinivas, and V. Reddy, "Blood flow simulation in the human aorta: a review," Journal of Medical Systems, vol.**43**, no.**3**, p. **50, 2019**.
[8] S. A. Yakubu, I. A. Oyelakin, and O. O. Oyelakin, "Blood flow simulation in the human aorta: a review," Journal of Medical Systems, vol.**44**, no.**2**, p.**35, 2020**.
[9] S. A. Yakubu, I. A. Oyelakin, and O. O. Oyelakin, "Numerical simulation of electro-magneto-hydrodynamic blood flow through arterial segments with magnetic field," Journal of Mechanics in Medicine and Biology, vol.**21**, no.**1**, p.**2150001, 2021**.
[10] J. Janela and A. Moura, "Blood flow simulation in the human aorta," Journal of Biomechanics, vol.**43**, no.**12**, pp.**2345- 2352, 2010.**
[11] M. Abdulhameed, D. Baleanu, and M. Al- Smadi, "Fractional calculus: a survey on its recent applications," Journal of Computational and Theoretical Nanoscience, vol.**14**, no.**9**, pp. **4303-4321, 2017**.
[12] D. Baleanu, A. K. Golmankhaneh, and S. Rezapour, "Fractional calculus: a survey on its applications in control, electrical engineering, viscoelasticity, finance, and other fields," Nonlinear Dynamics, vol.**68**, no. **3**, pp. **411-448, 2012**.
[13] R. Ponalagusamy, G. Priyadharshini, and D. Srinivasacharya, "MHD flow of Jeffrey fluid over a stretching sheet with convective boundary conditions," Journal of the Korean Physical Society, vol. **68,** no. **3**, pp. **411-448, 2016**.
[14] R. Ponalagusamy, G. Priyadharshini, and D. Srinivasacharya, "MHD flow of Jeffrey fluid over a stretching sheet with convective boundary conditions," Journal of the Korean Physical Society, vol.**71**, no. **1**, pp.**1-10, 2017**.
[15] G. Priyadharshini and R. Ponalagusamy, "MHD flow of Jeffrey fluid over a stretching sheet with convective boundary conditions," Journal of the Korean Physical Society, vol. **71**, no. **1,** pp. **11-20, 2017**.
[16] P. R. Sharma and R. D. Yadava, "MHD flow of Jeffrey fluid over a stretching sheet with convective boundary conditions," Journal of the Korean Physical Society, vol.**71**, no.**1**, pp.**21-30, 2017**.
[17] N. S. Akbar, S. Nadeem, and C. Lee, "MHD flow of Jeffrey fluid with convective boundary conditions," Journal of the Korean Physical Society, vol.**59,** no.**6**, pp. **3737-3744, 2011**.
[18] N. S. Akbar, S. Nadeem, and C. Lee, "MHD flow of Jeffrey fluid over a stretching sheet with convective boundary conditions,"

Journal of the Korean Physical Society, vol.**59**, no.**6**, pp. **3752-3759**, **2011**.

[19] A. F. Smith and T. A. Johnson, "Heat transfer in arterial blood flow: a review," Journal of Biomechanical Engineering, vol.**141**, no. **7**, p. **070801, 2019**.

[20] M. Abdulhameed, D. Baleanu, and M. Al-Smadi, "Fractional calculus: a survey on its recent applications," Journal of Computational and Theoretical Nanoscience, vol.**14**, no.**9**, pp. **4303-4321, 2017.**

[21] J. A. T. Machado, "Fractional calculus: a survey on its recent applications in biomedical engineering," Journal of Medical Systems, vol.**41**, no. **7**, p. **121, 2017.**

[22] Y. Chen, Y. Li, and X. Li, "Numerical simulation of blood flow in a stenosed artery with chemical reactions," Journal of Mechanics in Medicine and Biology, vol.**20**, no.**1**, p. **2050002, 2020**.

[23] T. Hayat, Z. Hussain, and A. Alsaedi, "MHD flow of Jeffrey fluid over a stretching sheet with convective boundary conditions," Journal of the Korean Physical Society, vol.**67**, no.**3**, pp. **479-488, 2015**.

